On-line biofouling monitoring and qualification based on local thermal and periodic excitation with MEMS sensor

Yassim Boukazia, Guillaume Delaplace, M. Cadé, F. Bellouard, L. Fillaudeau

On-line biofouling monitoring and qualification based on local thermal and periodic excitation with MEMS sensor

Y. BOUKAZIA[a,], G. DELAPLACE[b,c], M. CADÉ[d], F. BELLOUARD[e], L. FILLAUDEAU[a,f*]

a TBI, Université de Toulouse, CNRS UMR5504, INRAE UMR792, INSA, Toulouse, France

b INRAE, UR638, PIHM, Villeneuve d'Ascq, France

c UMET, CNRS-UMR8207, Université de Lille 1, Villeneuve d'Ascq, France

d Institut de Recherche Hydraulique (IRH), Ludres, France

e Aqualabo, Caudan, France

f FR FERMAT, Université de Toulouse, CNRS, INPT, UPS, Toulouse, France

* Corresponding Authors: Luc FILLAUDEAU and Yassim BOUKAZIA

Address: Toulouse Biotechnology Institute TBI (INSA/CNRS 5504, UMR INSA/INRA 792), 135 avenue de Rangueil 31077 Toulouse, France.

E-mail: luc.fillaudeau@insa-toulouse.fr or yassimboukazia@gmail.com

Table of content

Highlights

- Fouling monitoring with MEMS sensor based on periodic thermal excitation,
- Analysis of thermal spectral responses in periodic thermal regime,
- Identification of limits of detection and quantification under lab scale conditions,
- Transposition at pilot-plant scale was validated during domestic wastewater biofouling,
- In-situ quantification and qualification of fouling.

Keywords

fouling sensor, MEMS structure, periodic thermal excitation, spectral analysis, biofouling monitoring and qualification, wastewater application

Abstract

Water and wastewater processing (cooling tower, heat exchanger, treatment, etc.) generate desirable or undesirable biofouling (mineral, organic, biological) which may affect equipment or process performances. Fouling magnitude and nature stand as critical parameters to be evaluated in-situ and on-line to control and optimize the operation (production, cleaning).

A fouling sensor based on a Micro-Electro-Mechanical Systems (MEMS) structure generating a local in-situ periodic thermal excitation (PTR) was studied in order to quantify and qualify fouling. At lab scale, model deposit (PVC) were used to simulate fouling conditions. Limits of detection (LOD) and quantification (LOQ) under steady and periodic thermal regimes were compared. Transposition to industrial conditions was investigated at pilot-plant scale. A continuous bioprocess (PropellaTM reactor) was fed with diluted wastewater under controlled operating condition (temperature, mixing rate, flow rates, residence time) in order to mimic realistic industrial conditions and to generate a complex biofouling over six weeks. Thermal diffusivity, capacitive and resistive components are extracted from thermal spectrum response and a final fouling factor is introduced. Results demonstrate the ability to quantify and qualify a complex biofouling with in-situ and on-line information.

1. Introduction

In the current economic, industrial and environmental context, the use and control of water in the different systems is essential. Applications using water are vast, from the particular use (domestic water) as for public places, to agriculture (agricultural water) for the irrigation of the fields while passing by the industrial applications (industrial water). Proportions vary according to global location. Use in individuals and public places, requires a mastery of water treatment processes upstream and downstream of the use. Upstream to produce drinking water and downstream to reduce water pollution are regulated at national (Articles L210-1 and L211-1 of the Environment Code) and European (2004/35/CE directive) levels. The use of water is vital in agriculture to meet the different needs of crops and livestock. Mastering the quality of this water is fundamental. Electricity generation is the leading user of water in the industrial sector. Industrial applications requiring water are numerous (pharmaceutical, chemical, etc.) and for the vast majority require treatment to limit fouling development.

Fouling in industrial process and bioprocess can be described by unwanted particles accumulations on areas of a system (Awad, 2011). Epstein, 1983, firstly introduced the different fouling situations combining the five possible interfaces (gas-liquid, liquid-liquid, gas-solid, liquid-solid and gas-liquid-solid), and the five primary fouling categories (crystallization fouling including precipitation and solidification, particulate fouling-accumulation, chemical reaction fouling-deposit formation, corrosion fouling-accumulation and biological fouling-attachment of macroorganisms (macro-biofouling) and/or microorganisms (micro-biofouling or microbial fouling)). Wallhäußer et al, 2012, considering previous work, proposed a similar classification of fouling in food process context. Biological fouling or biofilm is generated by the development of microorganisms on the surface in contact with water, which is an ideal environment microorganism development (Batté et al.,

2003). The result of uncontrolled microbial growth on surfaces leads to biofouling formation due to aggregation of biological and non-organic materials. Microorganisms secrete polymers (polysaccharides and proteins), which adhere to surfaces. These polymeric substances extracellular are hydrated, that forming a gel network around microorganisms and contribute to integrity of biofilm. Gel may also incorporate non-biological components (organic or inorganic debris from various sources) into the biofilm polymer (Youssouf et al, 2016).

Magnitude (thickness) and characterization (nature) of fouling through *in-situ* and local sensors constitute technological and scientific challenges. Meantime, some sensors in industrial processes are sensitive to fouling development, which reduce sensitivity and degrade measurements (Marose et al., 1999; Scheper et al., 1996; Vojinović et al., 2006). The main laboratory and industrial techniques to monitor fouling have been reported by Fillaudeau et al, 2011, Crattelet et al, 2013, and updated by Boukazia, 2020. Various devices have been reported in the literature including rheological, electrical, chemical, mechanical, optical, sonic, ultrasonic, and thermal methods each exhibiting its own specificities, advantages and disadvantages (Duffau et al., 1991; Withers, 1996; Janknecht and Melo, 2003; Prakash et al., 2005; Wallhäußer et al., 2012). A classification (Fillaudeau et al, 2011) was proposed by considering multiple criterion: level of development (academic lab work, Industrial applications), operating mode (batch or continuous process), local and global measurement, intrusive and non-intrusive sensor, on-line or post-process analyze and direct or indirect thickness estimation. Considering industrial specifications, fouling information (quantification and qualification) must be obtained on-line, in real time and non-destructively and the sensor must be robust, easy to use and inexpensive.

Over the past two decades, alternative sensors based on hot wire technique have been scrutinized and validated as an accurate method for fouling monitoring. Crattelet et al. 2011 has investigated a thermal excitation generated by a sensitive element composed of a Micro-Electro-mechanical Systems (MEMS) technology. Boukazia et al, 2020 characterized the performances of three fouling sensors based on steady thermal regime (STR) and different technology (MEMS and macroscopic), geometry (flat and cylindric) and packaging. This recent work performed at lab scale leads to select an optimal structure under model fouling conditions.

In present work, a prototype thermal sensor (TS) including a sensitive element based on MEMS technology in flat geometry is investigated under periodic thermal excitation. The overarching aim of thermal spectrum analysis stand in the quantification and qualification of fouling. At lab scale, the sensor was characterized under controlled fouled conditions with model deposit (PVC tape). Limits of detection (LoD) and quantification (LoQ) under steady and periodic thermal regimes are compared. Then transposition to industrial conditions is scrutinized. Biofouling is generated and monitored under controlled conditions during domestic wastewater treatment in bioreactor (Propella^{TM}) over six weeks. Extraction of thermal diffusivity, capacitive and resistive components highlights about fouling kinetics, magnitude and nature and leads to propose a final fouling factor.

2. Materials and Methods

2.1. Sensors, operating and structure

2.1.1. Theory

The structure and operating principle of the sensor are described in patent n°FR2885694 (INRAE, France) and by (Boukazia et al., 2020). Sensor principle is based on differential thermal measurement (called hot wire). A heating element is used to impose and to measure a regulated heat flux with a constant value (steady thermal regime, STR) or a sinusoidal shape (periodic thermal regime, PTR) in established conditions. Then temperatures are measured at two different locations: into the hot wire element and into the bulk. Knowing these parameters and the structure of the sensor, the resolution of heat balance equation (Eq.1) permits to determine thickness and thermal properties of fouling.

$$q + \lambda \cdot \nabla\theta = \rho \cdot Cp \cdot \frac{\partial\theta}{\partial t} \qquad \text{(Eq.1)}$$

Where $\nabla\theta$ describes geometry of problem in Cartesian coordinates:

$$\nabla\theta = \frac{\partial^2\theta}{\partial x^2} + \frac{\partial^2\theta}{\partial y^2} + \frac{\partial^2\theta}{\partial z^2} \qquad \text{(Eq.2)}$$

In periodic thermal regime (PTR), following assumptions from Eq.1 are made to deduce Eq.3 (Crattelet et al., 2013; Khaled, 2008; Ould Lahoucine and Khellaf, 2004; Strub et al., 2005): (i) temperature variation with time ($\frac{\partial T}{\partial t} \neq 0$), (ii) no heat generation ($q = 0$), (iii) one-dimensional following x axis (z = y = 0) and perfect thermal insulation on back side ($\varphi_{eff} = \varphi_{nom}$) .

$$\Delta\theta_{PTR}(x,t) = Rth \cdot \Delta\theta_A \cdot exp\left(-\sqrt{\frac{\omega}{2a}}x\right) \cdot cos(\omega t + \Delta\phi) + Rth \cdot \varphi_C \qquad \text{(Eq.3)}$$

As in electrical domain, an alternating ($\Delta\theta_P(x,t)$) and a continuous component ($\Delta\theta_C(x)$) can be identified in the temperature difference signal:

$$\Delta\theta_{PTR}(x,t) = \Delta\theta_P(x,t) + \Delta\theta_C(x) \begin{cases} \Delta\theta_P(x,t) = \Delta\theta_A \cdot cos(\omega t + \Delta\phi) \\ \Delta\theta_C(x) = Rth \cdot \varphi_C \end{cases} \quad \text{(Eq.4)}$$

Where *A* is the amplitude of temperature signal and $\Delta\phi$ the phase lag:

$$\Delta\theta_A = Rth \cdot \varphi_A \cdot exp\left(-\sqrt{\frac{\omega}{2a}}x\right) \quad \text{(Eq.5)}$$

$$\Delta\phi = -\sqrt{\frac{\omega}{2a}}x \quad \text{(Eq.6)}$$

PTR analysis enables to determine both thermal resistance and diffusivity of fouling corresponding to its resistive and capacitive components respectively. Thermal resistance is deduced from the continuous component (mean value) whereas amplitude leads to extract thermal resistance and diffusivity. The phase lag give access to thermal diffusivity.

2.1.2. Sensors structure

Figure 1 illustrates the structure (A) and picture (B) of sensor. The thermal sensor is composed of a flat square MEMS structure on a silica wafer (red wire, thickness = 250 nm) stuck on a printed circuit board PCB (green line) in contact with bulk. On the silica wafer surface, a platinum wire (hot wire) has been deposited and covers an active area about 4x4 mm² and a thickness of 190 nm. The hot wire allows a heat flux range of 250 to 7500 W m^{-2} (with P < 120 mW) and a temperature accuracy measurement of ±0.1 K. The PCB is a classic disk of 11.5 mm diameter and 800 µm thickness. The protective packaging is composed of a stainless steel cylinder (diameter 15.5 mm) fill with thermally conductive resin layers. A thermo-resistance NTC probe (blue half circle) measured the bulk temperature. TS1 can operate with flush or intrusive positions into the process. Absence of protective packaging reduce the acceptable operating conditions applicative (4 < pH < 10, < 353.15 K, P <3 bar, fluid without hard particles in suspension).

Figure 1C represents the data acquisition chain. Connected to the sensitive element, the conditioning card performs the filtering and amplification of the signals. Then the acquisition

card samples the signals with a defined frequency (1 Hz < $f_{sampling}$ < 10 Hz). Low frequency is adapted to thermal sensors and their thermal inertia (t_{resp} < 10 s, (Boukazia et al., 2020)). The card is connected to the Digital Module Modbus provided by Aqualabo (Caudan, France) and consists of a communication bus (allowing monitoring of several sensors). Data are recorded to the computer through an electrical box powered with 7 and 230 V.

2.2. Laboratory scale

2.2.1. Experimental setup and model deposits

The experimental setup is composed of two elements, a mixed reactor and a derivation loop in order to mitigate operating conditions in batch and continuous processes (Boukazia et al., 2020). In lab set-up, PVC adhesive tape (TESA® 53948, thickness = 130 µm, ρ = 1300 kg·m^{-3}) was used to mimic fouled conditions. Thermal conductivity and heat capacity were measured at λ = 0.115 W·m^{-1}·K^{-1} and at Cp = 1025 J·K^{-1}·kg^{-1} for PVC adhesive tape (Neotim FP2C, 0.02 to 5 W·m^{-1}·K^{-1}, 5 %, France). PVC adhesive tape thicknesses were controlled at 140 ± 10 µm with an automatic microscope (Malvern, Morphologi G3S-ID, United Kingdom) using focus stacking method (Kibby, 2019).

2.2.2. Experimental protocol

In PTR, a periodic sinusoidal heat flux was applied with minimal and maximal values of 630 and 8800 W·m^{-2} corresponding to φ_C = 4715 W·m^{-2} and φ_A = 4085 W·m^{-2} respectively. The frequency was modulated from 0.001 to 0.2 Hz (8 frequencies). Data were recorded during at least three periods for all experimental conditions.

Under clean condition, measurements were performed as reference state under defined flow regime. Under fouled conditions, two series were performed with PVC tape with 5 (0 to 700 µm ± 50 µm) and 9 (0 to 1260 µm ± 90 µm) successive layers respectively. STR and PTR

responses are scrutinized and sensitivity, limits of detection and quantification can be determined. Thermal spectral responses for amplitude and continuous component are analyzed to extract the thermal diffusivity, resistive and capacitive components.

2.3. At pilot-plant scale

2.3.1. Propella™ setup

The pilot-plant (Figure 2) is operating in continuous mode and includes three main parts: (i) a feed tank, (ii) a Propella™ bioreactor and (iii) drain. The feeding section is composed of a 30 L mixed tank (Euro-STD, 50 to 2000 RPM) and one multi-parameter (MP) instrument. Dissolved oxygen (pO_2), pH and electrical conductivity (σ) are measured by OPTOD (PF-CAP-C-00141, AQUALABO, 0 to 20 ± 0.1 mg·L^{-1}, France), PHEHT (PF-CAP-C-00345, AQUALABO, 0 to 14 ± 0.1, France) and C4E (PF-CAP-C-00150, AQUALABO, 0 to 2000 µS·cm^{-1}, France) respectively. All data are recorded through acquisition equipment ODEON (NC-POR-C-00133, AQUALABO, France). The feed tank is filled with wastewater through the pump (GALA1000PPE200UA002000, ProMinent, 0.74 L·h^{-1}, Germany).

Propella™ bioreactor (Appenzeller et al., 2001; Gosselin et al., 2013; Ilkka Miettinen, 2005; Manuel, 2007; Mathieu et al., 2019) is a 3 L reactor (D_{int} = 93.4 mm, h = 500 mm). Effluent is pushed downstream into an internal cylinder (D_{ext} = 72.5 mm, D_{int} = 44 mm, *h-tube* = 460 mm) by a propulsive propeller (3 blades marine impeller) driven by motor (Euro-STD, 50 to 2000 RPM). Along the outer cylinder (annular space) are located 20 connecting drills to install the coupons (material test) and thermal sensor. Temperature regulation is ensured by a cryostat (GD120, Grant, 0 to 120 ± 0.02 °C, England) via water circulation in an external loop and inside the internal cylinder. In bioreactor, the inlet and outlet wastewater are located on the top and bottom of bioreactor. The average hydraulic residence time, $\tau = \frac{V}{Q}$ is

determined by feeding flowrate. The wastewater ascends between inner and outer wall. Flow regime (Reynolds number) in annular space is controlled by pumping effect of mixing rate (Manuel, 2007).

The last part drains the effluent out of the experimental set-up by the bottom of Propella™ bioreactor. Fluid level is adjusted by the height of the overflow with a venting.

Coupons are in contact with fluid inside Propella™ reactor. They are stuck to cylindrical mechanical supports and several gaskets ensure sealing. Coupons materials were stainless steel and MEMS chips (same dimension). The system for extracting coupon includes a valve, a tool and a coupon rack in order to ensure waterproofing during their positioning and removing.

2.3.2. Experimental protocol

Pilot-plant experiments aim to validate in-situ fouling measurement under realistic industrial conditions during the formation and elimination of complex biofouling formation and elimination. Feeding tank was filled, every two days, with fresh domestic wastewater (Veolia eau Ginestou), the inlet of wastewater from treatment plant was diluted with outlet water to adjust sludge concentration. Effluent concentration was gradually increased from 20 % to 40 % and 80 % every two weeks. In the feed tank, the mixing rate was set at 100 RPM without temperature regulation (room temperature between 14 and 20 °C). Feeding flowrate was regulated at 50 % of piston-pump corresponding to 200 $mL \cdot h^{-1}$. Bioreactor temperature was regulated at 37 °C by using a thermostat (GD120, Grant, 0 to 120 ± 0.02 °C, England) via water circulation in an external duct and in the inner cylinders. The mixing rate was adjusted to 350 RPM, equivalent to Re = 1000 ± 100 within annular space (Manuel, 2007). This laminar flow regime induced a low heat convection coefficient at the sensor surface (Armstrong et al., 2017).

After six weeks, two cleaning steps were performed. The first phase consisted in washing experimental set-up with 10 L of diluted hypochlorite solution (0.1 % active chloride) during 24 h. A second phase consisted in adding a pulse of concentrated hypochlorite (50 mL, 9.6 % active chloride) directly into the bioreactor.

Measurements with fouling sensors were performed three times per week in STR and PTR. In STR, five heat flux slots were applied (from 260 to 7500 $W \cdot m^{-2}$) during 10 min per slot (measurement phase of 60 min). In PTR, measuring conditions were similar to lab scale experiments.

3. Results and discussion

3.1. Systemic study at laboratory scale: from raw data to fouling quantification and qualification

3.1.1. Raw data in periodic thermal regime (PTR)

Figure 3A illustrates raw data acquisition, heat flux, (φ) and temperature differences ($\Delta\vartheta$) during two periods ($f = 0.001\ Hz, \varphi_C = 4700\ W \cdot m^{-2}, \varphi_A = 4100\ W \cdot m^{-2}$). Considering clean ($Rth = 0$ K·W^{-1}) and fouled (Rth = 353 K·W^{-1}) conditions, the amplitudes ($\Delta\vartheta_A$) and mean temperature differences ($\Delta\vartheta_C$) increase from 0.7 to 4.2 K and from 1 to 5.2 K respectively. Figure 3B shows a concatenation of each frequency (from 0.001 to 0.2 Hz) for temperature differences, $\Delta\vartheta$ in clean and fouled conditions (Rth = 353 K·W^{-1}). As expected, $\Delta\vartheta_A$ decrease whereas $\Delta\vartheta_C$ remain constant with rising frequency. To discuss results, variation coefficients of raw data are treated.

Firstly, all thermal signals are filtered at 0.001 Hz through the Butterworth Filter of LabVIEW (National Instrument), to remove noise generated by high frequency phenomena. The differences between raw and filtered signals are determined to evaluate the root mean square (RMS) of noise. The RMS of noise decrease from 0.09 to 0.04 K under clean and fouled conditions respectively. These values are consistent with sensor specification. The variation coefficient (RMS of noise divided by thermal amplitude component, $\Delta\vartheta_A$) decrease with fouling magnitude from 12.7 to 1.1 % in PTR. A decrease of the variation coefficients, from 1 to 0.01 % in STR was previously reported for similar conditions (Boukazia et al., 2020).

3.1.2. Thermal spectrum analysis and extraction of thermal properties

Considering raw data and equation Eq.5, the frequency spectrum of amplitude ($\Delta\vartheta_A$) and mean temperature differences ($\Delta\vartheta_C$) are plotted as a function of angular velocity square root, $\omega^{½}$ for clean and fouled conditions (Figure 4A and Figure 4B). Considering mean temperature differences ($\Delta\vartheta_C$) and knowing the mean continuous heat flux, φ_C then resistive component of deposit, $Rth = {}^{th}/_{\lambda}$ is extracted : $\Delta\theta_C(x) = Rth \cdot \varphi_C$ (Eq.4).

Thermal amplitude, $\Delta\vartheta_A$ decreases with frequency and amplifies with the fouling thermal resistance. The continuous component ($\Delta\vartheta_C$) increases with fouling magnitude, but it is independent of frequency as reported in Table 1.

The thermal amplitude, $\Delta\vartheta_A$ evolution versus frequency is modeled by analytical expression (Eq.5) with an exponential function ($\Delta\theta_A = \beta \cdot exp(\alpha)$), thus, $\alpha = -\sqrt{\frac{1}{2a}}x \; and \; \beta = Rth \cdot \varphi_A$ are identified (Table 1). Knowing the amplitude of heat flux excitation, φ_A, the resistive components of deposit, $R_{th} = {}^{th}/_{\lambda}$ can be deduced. Then the capacitive component of deposit, $Cth = \rho \cdot Cp \cdot th$ (where $x = th$) is determined from parameter α including fouling thickness and thermal diffusivity. Conductive and capacitive components inform about the magnitude of fouling phenomena and the thermal properties. Thermal effusivity, $E = \sqrt{\rho \cdot Cp \cdot \lambda}$ corresponds to the ratio of capacitive and conductive components.

3.1.3. Thermal resistive and capacitive components of deposit

3.1.3.1. Thermal resistance, Rth

Thermal resistance, *Rth* can be obtained in STR (Boukazia et al., 2020) and PTR considering amplitude, mean heat flux and temperature differences (Eq.4 and Eq.5). Figure 5A reports the evolution of experimental thermal resistances extracted from thermal amplitude (PTR_A) and mean continuous values (PTR_C) as a function of theoretical thermal resistance. Inflexions

of experimental thermal resistances are noticeable for the highest fouling. It highlights edges and backside effects. Under the same conditions, (Boukazia et al., 2020) determined the thermal resistances, *Rth* in STR by a linearization of thermal differences as a function of heat flux ($250 < \varphi_{STR} < 7500$ W·m^{-2}). As shown in Figure 5A, STR and PTR_C ($\varphi_{PTR\text{-}C} = 4700$ W·m^{-2}) data are compared and exhibit similar trends and values. PTR_A (with $\varphi_{PTR\text{-}A} = 4100$ W·m^{-2}) data are closer to linearity indicating a more reliable estimation of thermal resistance even if a higher noise was observed on raw data. Table 2 indicates the relative deviations between STR and PTR (mean continuous and amplitude) for thermal resistances. As expected, mean relative error decreases with fouling magnitude and remains close (< 2.8%) between STR and PTR_C. A high degree of confidence is noticeable under PTR_C whereas thermal resistance was determined with only one heat flux ($\varphi_{PTR\text{-}C} = 4700$ W·m^{-2}). Relative error between STR and PTR_A decreases slightly with fouling magnitude, but it remains close to 15 %. Improved performances may be attributed to excitation mode. In addition, amplitude of PTR signal may be the most efficient (less sensitive of heat loss).

Based on a minimal thermal deviation of 0.2°C, the lowest detectable thermal resistances (min LOD) are equal to 1.47E-4 and 1.69E-4 K·m^2·W^{-1} for PTR_C and PTR_A respectively. The corresponding thicknesses for a dense biofouling ($\lambda_{bio} = 0.6\ W \cdot m^{-1} \cdot K^{-1}$) are estimated to 88 and 101 µm for PTR_C and PTR_A respectively. Considering a maximum deviation of 30 % (industrial specification) to linearity, the upper LOD can be estimated at 3.32E-3 and 5.05E-3 K·m^2·W^{-1} for PTR_C and PTR_A respectively. Comparing to a dense biofouling, equivalent thicknesses are equal to 2.0 and 3.0 mm for PTR_C and PTR_A respectively. These ranges of detection are consistent with industrial specifications (biofilm < 2 mm, precision superior to 30%) for water treatment, air-cooling tower and bioprocess. In STR, lower and upper LOD equal to 54.6 and 2140 µm with higher heat flux (7600 W·m^{-2}) and linearized flux-

temperature curves were reported (Boukazia et al., 2020). In PTR, the metrological performances were achieved by dissipated 50% of STR power. In present case, the mean and/or amplitude of heat flux could be increase to improve the lower LOD in PTR_C and PTR_A. Considering a polynomial regression and coefficients errors, the limit of quantification (LOQ) is estimated to 1.1E-7 and 1.7E-7 $K{\cdot}m^2{\cdot}W^{-1}$ for PTR_C and PTR_A respectively. Beyond the limit of 30 %, the inflexion of sensor response is noticeable. However thermal resistance can be estimated in a degraded mode up to 1.02E-2 $K{\cdot}m^2{\cdot}W^{-1}$ (equivalent to 6.1 mm).

3.1.3.2. Thermal diffusivity and capacitive component

Considering the parameter α and knowing the PVC tape thickness, the thermal diffusivity of material can be estimated and compared with literature. Figure 5B describes the evolution of PVC thermal diffusivity as a function of deposit thickness. A constant value is observed with thickness inferior to 400 µm which is equivalent to thermal resistance close to 3.5E-3 $m^2{\cdot}K{\cdot}W$ (LOD max). The average thermal diffusivity of deposit is then estimated to 8.59E-8 $m^2{\cdot}s^{-1}$, which appears consistent with literature (Lide, 2003) mentioning α_{PVC} = 8.63E-8 $m^2{\cdot}s^{-1}$. For higher thickness, the estimated thermal diffusivity sharply increases in agreement with metrological limits and signal saturation of fouling sensor. We assumed that heat loss on backside and edge become the dominant phenomena.

The knowledge of *Rth* and α leads to determine the thermal capacitive component, $C_{th} = \rho \cdot C_p \cdot th$ as shown in Figure 5B. Up to 400 µm, it evolves linearly with thickness. Beyond 400 µm, the same inflexion is noticeable and may be attributed by metrological limits of sensor.

3.2. Biofouling monitoring at pilot-plant scale: application to domestic wastewater treatment

Prototype fouling thermal sensor should be transposed from lab to semi-industrial conditions and validated into bioprocess with industrial realistic conditions. Fouling monitoring was performed during treatment of domestic wastewater in a Propella™ bioreactor (Appenzeller et al., 2001; Gosselin et al., 2013; Mathieu et al., 2019). The objectives were to monitor the kinetics associated with the formation and elimination of deposit, to estimate its propensity and to qualify its thermal properties thanks to in-situ and local measurements.

3.2.1. Fouling quantification, *Rth* in STR and PTR.

Operating conditions were controlled and physicochemical parameters of wastewater were monitored. Temperature and electrical conductivity of fluid have evolved from 14 to 18 °C and from 700 to 1000 $\mu S \cdot cm^{-1}$ respectively. Electrical conductivity values increased with wastewater concentration (699 $\pm$ 12, 741 $\pm$ 45 and 940 $\pm$ 21 $\mu S \cdot cm^{-1}$ for 20, 40 and 80 % respectively). pH remained constant around 7.0 $\pm$ 0.19. Flowrate was controlled every 2 days during the campaign at 200 ± 50 $mL \cdot h^{-1}$ ($12 < \tau < 20$ h in Propella™ reactor). Temperature inside Propella™ reactor was reported from bulk measurement of TS and evolved from 30 to 36 °C. Operating conditions were accurately controlled along the experiments for this type of bioprocess.

Responses from fouling sensor can be analyzed in STR and PTR. Figure 6 compares the thermal resistances as a function of time including feed concentration (20, 40 and 80 %) and two cleaning steps (1 and 2). During the first 20 days, fluctuation of thermal resistances is observed followed by a constant increase up to the 41st day. Variations of thermal resistances may be explained by the balance between the formation and detachment of a

fragile deposit at sensor surface under dilute conditions. For both excitation modes, STR and PTR, the increases of thermal resistances enlightened the fouling kinetics with successive phases.

Ex-situ images of MEMS coupons (magnification: x2.5, x10 and x50) after five weeks are illustrated in Figure 7. Fouling has settled on both platinum and silica part without distinction and confirm impact of fouling on sensor results. However, these observations revealed an underestimated fouling and did not permit an ex-situ quantification. This limited fouling could be explained by the protocol to remove coupons. Before microscopic observations, coupons are manually removed from the reactor (including mechanical shocks), conditioned (cleaning, immersed in water) and transportation to the laboratory. These steps generated mechanical stresses and vibrations and highly reduced an initial fragile and heterogeneous deposit. Alternative way should be developed to cross-checked in-situ measurements with fouling sensor.

In-situ thermal resistances increase up to 1.73E-3, 1.59E-3 and 1.75E-3 $K{\cdot}m^2{\cdot}W^{-1}$ for STR, PTR_C and PTR_A respectively. These values correspond to equivalent biofouling thicknesses around 1040, 950 and 1050 µm ($\lambda_{bio} = 0.6\, W \cdot m^{-1} \cdot K^{-1}$) for STR, PTR_C and PTR_A respectively. Finally, thermal resistances decrease during cleaning phases as expected. However, chemical shocks are not sufficient to ensure the full recovery of clean sensor surface.

3.2.2. Fouling characterization in PTR

In PTR, the capacitive and conductive components are extracted and presented in Figure 8. Results from lab scale (PVC adhesive tape) and data from literature for magnesium silicate ($MgSiO_3$), water and PVC are also reported (Akaogi and Ito, 1993; Haigis et al., 2012). Thermal capacitive ($\rho{\cdot}Cp{\cdot}th$) and resistive ($th{\cdot}\lambda^{-1}$) components evolve linearly as a function of

the thickness of deposit. The fouling vector modulus, $|F| = th \cdot \sqrt{(\rho \cdot Cp)^2 + \left(\frac{1}{\lambda}\right)^2}$ informs about fouling magnitude (associated with kinetics) and the angle (slope) about the nature of deposit. The slope is equal to the square of thermal effusivity, $E^2 = \rho \cdot Cp \cdot \lambda$. Regarding experimental results with PVC tape and biofouling, two mean slopes are clearly distinguished with thermal effusivity equal to 418 and 821 $J \cdot s^{0.5} \cdot K^{-1} \cdot m^{-2}$ respectively. With PVC thermal effusivity remains constant as deposit nature does not evolve. On the opposite with wastewater treatment, a slope inflexion may indicate a significant time-evolution of fouling nature through its thermal properties.

A final fouling factor, *FFF* (Eq.7) can be introduced as a qualitative indicator to report about deposit nature (organic / mineral) based on its thermal properties.

$$FFF = \frac{ln(E_{exp}) - ln(E_{min})}{ln(E_{max}) - ln(E_{min})} \quad \text{(Eq.7)}$$

In present case, magnesium silicate ($MgSiO_3$) and PVC were considered as minimum (0%) and maximum (100%) references. Thermal effusivity was extracted from literature (Akaogi and Ito, 1993; Haigis et al., 2012) for $MgSiO_3$ (E_{max}= 4041 $J \cdot s^{0.5} \cdot K^{-1} \cdot m^{-2}$), water ($E_{water}$= 1586 $J \cdot s^{0.5} \cdot K^{-1} \cdot m^{-2}$) and PVC ($E_{min}$= 391 $J \cdot s^{0.5} \cdot K^{-1} \cdot m^{-2}$). Considering experimental results, *FFF* values are equal to 3.1 and 29.5 % for PVC deposit and wastewater biofouling respectively. As expected, FFF_{PVC} is close to the theoretical value of PVC. Whereas for biofouling, $FFF_{wastewater}$ is highly superior and closer to the slope of water. Thus, FFF is considered as a useful and precious indicator to be associated with fouling magnitude estimation. However, the deposit generated into Propella™ bioreactor is largely unknown and assumes to be a complex biofouling (organic, mineral and biological matter).

The ability to discriminate the fouling by considering thermal capacitive and conductive properties of different materials (organic, mineral, and biological) can be assumed for long

processes through in-situ measurements. At present time, the periodic excitation used in this study needs 2 h (eight frequencies and three periods), which is adapted for slow fouling kinetics and long duration industrial process (from days to months). A simplified PTR can be defined by reducing the number of frequencies (four frequencies: 0.002, 0.008, 0.04 and 0.2 Hz) and recording one period. Then simplified PTR measurements would be suitable for fast fouling kinetics and achieved within 10 minutes. However, for short or instantaneous phenomena (chemical cleaning, mechanical deposit removal), STR excitation would be privileged, but the response time of sensor should considered (Boukazia et al., 2020).

4. Conclusion

A prototype fouling sensor based on a Micro-Electro-Mechanical Systems (MEMS) structure and generating a local in-situ periodic thermal excitation (PTR) was scrutinized and characterized at lab and pilot-plant scales to quantify and qualify in-situ fouling.

At lab scale, the metrological performances (LoD, LoQ) were determined with model deposit to mimic fouled conditions. In PTR, continuous and amplitude components of thermal spectrum were used to extract thermal resistance and compared with STR. The systemic approach demonstrates that PTR exhibits better metrological performances than STR. Limits of detection can be improved with a higher heat flux. Analytical expression of spectral responses leads to extract information about the deposit magnitude and its thermal properties. Considering the frequency spectrum of thermal amplitude and the fouling thickness, the thermal diffusivity was calculated and appeared consistent with literature.

At pilot-plant scale, the transposition to industrial conditions was validated. A continuous bioprocess (PropellaTM reactor) was fed with diluted wastewater under controlled operating conditions (temperature, mixing rate, flowrates and residence time) to mimic realistic industrial conditions and to generate a complex and evolving biofouling over six weeks. Thermal diffusivity, capacitive and resistive components were extracted from thermal spectrum response. A final fouling factor was introduced to qualify deposit while fouling propensity is given by the modulus of fouling vector. Results demonstrated the ability to quantify and qualify a complex biofouling with in-situ and on-line information. However, in-situ measurements with fouling sensors should be confronted to other methods. Finally, PTR could be optimized (frequencies, period) in order to reduce the duration of measurement cycle. Long measurement time will be adapted for slow fouling kinetics as encountered in numerous industrial processes (air cooling tower, wastewater treatment).

ACKNOWLEDGEMENTS

Authors are grateful to CAPENC project (FUI AAP16, n°F1311001L) funded by BPI France, involving academic and industrial partnership (AQUALABO, VERI, IRH, TBI). We thank M. Marc BEGUE (LMDC, INSA Toulouse) for his help with thermal conductivity and heat capacity characterization.

Nomenclature

a	Thermal diffusivity	$[m^2 \cdot s^{-1}]$
Cp	Specific heat capacity	$[J \cdot kg^{-1} \cdot K^{-1}]$
Cth	Capacitive component	$[J \cdot K^{-1} \cdot m^{-2}]$
D	Diameter	[m]
E	Thermal effusivity	$[J \cdot s^{0.5} \cdot K^{-1} \cdot m^{-2}]$
FFF	Finale Fouling Factor	[%]
f	Frequency	[Hz]
h	Heat coefficient convection	$[W \cdot m^{-2} \cdot K^{-1}]$
Q	Flow	$[mL \cdot h^{-1}]$
q	Volume heat generation	$[W \cdot m^{-3}]$
t	Time	[s]
t_{resp}	Response time	[s]
th	Thickness	[m]
Re	Reynold number	[/]
Rs	Surface thermal resistance	$[K \cdot m^2 \cdot W^{-1}]$
Rth	Thermal resistance	$[K \cdot W^{-1}]$
V	Volume	$[m^3]$
x, y, z	Dimension	[m]

Greek letter

θ	Temperature	[K]
Δθ	Temperature difference	[K]
Δϕ	Phase lag	[rad]
λ	Thermal conductivity	$[W \cdot m^{-1} \cdot K^{-1}]$
μ	Viscosity	[Pa·s]
ν	Speed	$[m \cdot s^{-1}]$
ρ	Density	$[kg \cdot m^{-3}]$
σ	Electrical conductivity	$[\mu S \cdot cm^{-1}]$
τ	Holding time	$[h^{-1}]$
φ	Heat flux	$[W \cdot m^2]$
ω	Angular velocity	$[rad \cdot s^{-1}]$

Indices

A	Amplitude
b	Bulk
C	Continuous component
ext	External
exp	Experimental
int	Internal
P	Periodic component

PTR	Periodic Thermal Regime
sampling	Sampling
theo	Theoretical

References

Akaogi, M., Ito, E., 1993. Heat capacity of MgSiO3 perovskite. Geophysical Research Letters 20, 105-108.

Akiyama, T., Ohta, H., Takahashi, R., Waseda, Y., Yagi, J.-i., 1992. Measurement and Modeling of Thermal Conductivity for Dense Iron Oxide and Porous Iron Ore Agglomerates in Stepwise Reduction. ISIJ International 32, 829-837.

Appenzeller, B.M.R., Batté, M., Mathieu, L., Block, J.C., Lahoussine, V., Cavard, J., Gatel, D., 2001. Effect of adding phosphate to drinking water on bacterial growth in slightly and highly corroded pipes. Water Research 35, 1100-1105.

Armstrong, R.C., 2017. Fluid mechanics and heat transfer. Heat Exchanger Design Handbook.

Awad, M.M., 2011. Fouling of Heat Transfer Surfaces, in: Belmiloudi, A. (Ed.), Heat Transfer.

Batté, M., Appenzeller, B.M.R., Grandjean, D., Fass, S., Gauthier, V., Jorand, F., Mathieu, L., Boualam, M., Saby, S., Block, J.C., 2003. Biofilms in Drinking Water Distribution Systems. Reviews in Environmental Science and Biotechnology 2, 147-168.

Boukazia, Y., Delaplace, G., Cadé, M., Bellouard, F., Bégué, M., Semmar, N., Fillaudeau, L., 2020. Metrological performances of fouling sensors based on steady thermal excitation applied to bioprocess. Food and Bioproducts Processing 119, 226-237.

Boukazia, Y., 2020. Development of in-situ physical metrology of fouling in industrial bioprocesses - Characterization and modelling of thermal and electrical responses of sensitive elements (MEMS) and prototype sensors. PhD thesis, INSA Toulouse, France.

Crattelet, J., Fillaudeau, L., Auret, L., Salvagnac, L., Boukabache, A., Estève ,D, 2011. Micro-capteur pour la mesure en ligne et en continu de l'encrassement dans les procédés industriels et de traitement de l'eau : Réalisation et caractérisation du microsystème. Instrumentation, Mesure, Métrologie 11, 107-130.

Crattelet, J., Ghnimi, S., Debreyne, P., Zaid, I., Boukabache, A., Esteve, D., Auret, L., Fillaudeau, L., 2013. On-line local thermal pulse analysis sensor to monitor fouling and cleaning: Application to dairy product pasteurisation with an ohmic cell jet heater. Journal of Food Engineering 119, 72-83.

Davies, T.J., Henstridge, S.C., Gillham, C.R., Wilson, D.I., 1997. Investigation of Whey Protein Deposit Properties Using Heat Flux Sensors. Food and Bioproducts Processing 75, 106-110.

de Beer, D., Stoodley, P., Lewandowski, Z., 1997. Measurement of local diffusion coefficients in biofilms by microinjection and confocal microscopy. Biotechnology and Bioengineering 53, 151-158.

Delplace, F., Leuliet, J.C., Tissier, J.P., 1994. Fouling experiments of a plate heat exchanger by whey proteins solutions. Food and bioproducts processing 72.

Fillaudeau, L., Crattelet, J., Auret, L., 2011. Fouling monitoring using differential thermal analyse under steady and periodic heat flow. Encyclopedia of Agricultural, Food and Biological Engineering, 1-11.

Epstein N, 1983. Thinking about Heat Transfer Fouling: A 5 × 5 Matrix. Heat Transfer Engineering, 43-56.

Flemming, H.C., 1991. Biofouling in Water Treatment, in: Flemming, H.-C., Geesey, G.G. (Eds.), Biofouling and Biocorrosion in Industrial Water Systems. Springer Berlin Heidelberg, Berlin, Heidelberg, pp. 47-80.

Flint, S., Bremer, P., Brooks, J., Palmer, J., Sadiq, F.A., Seale, B., Teh, K.H., Wu, S., Md Zain, S.N., 2020. Bacterial fouling in dairy processing. International Dairy Journal 101, 104593.

Gosselin, F., Madeira, L.M., Juhna, T., Block, J.C., 2013. Drinking water and biofilm disinfection by Fenton-like reaction. Water Research 47, 5631-5638.
Guinea, A., Playà, E., Rivero, L., Ledo, J.J., Queralt, P., 2012. The electrical properties of calcium sulfate rocks from decametric to micrometric scale. Journal of Applied Geophysics 85, 80-91.
Haigis, V., Salanne, M., Jahn, S., 2012. Thermal conductivity of MgO, MgSiO3 perovskite and post-perovskite in the Earth's deep mantle. Earth and Planetary Science Letters 355–356, 102-108.
Ilkka Miettinen, G.S., 2005. Surveillance and control of microbiological stability in drinking water distribution networks.
Inaba, H., Miyahara, K., Naito, K., 1984. Measurement of the molar heat capacities of MoO2 and MoO3 from 350 to 950 K. The Journal of Chemical Thermodynamics 16, 643-651.
Khaldi, M., Blanpain-Avet, P., Guérin, R., Ronse, G., Bouvier, L., André, C., Bornaz, S., Croguennec, T., Jeantet, R., Delaplace, G., 2015. Effect of calcium content and flow regime on whey protein fouling and cleaning in a plate heat exchanger. Journal of Food Engineering 147, 68-78.
Khaled, A.R.A., 2008. Conduction heat and entropy transfer in a semi-infinite medium and wall with a combined periodic heat flux and convective boundary condition. International Journal of Thermal Sciences 47, 76-83.
Kibby, G., 2019. Focus stacking in macrophotography and microphotography. Field Mycology 20, 51-54.
Kumar, C.G., Anand, S.K., 1998. Significance of microbial biofilms in food industry: a review. International Journal of Food Microbiology 42, 9-27.
Ličina, V., Moguš-Milanković, A., Reis, S.T., Day, D.E., 2007. Electronic conductivity in zinc iron phosphate glasses. Journal of Non-Crystalline Solids 353, 4395-4399.
Lide, D.R., 2003. Handbook of Chemistry and Physics.
Manuel, C.M.D., 2007. Biofilm dynamics and drinking water stability : effects of hydrodynamics and surface materials.
Marose, S., Lindemann, C., Ulber, R., Scheper, T., 1999. Optical sensor systems for bioprocess monitoring. Trends in Biotechnology 17, 30-34.
Mathieu, L., Keraval, A., Declercq, N.F., Block, J.-C., 2019. Assessment of a low-frequency ultrasound device on prevention of biofilm formation and carbonate deposition in drinking water systems. Ultrasonics Sonochemistry 52, 41-49.
Notermans, S., Dormans, J.A.M.A., Mead, G.C., 1991. Contribution of surface attachment to the establishment of micro-organisms in food processing plants: A review. Biofouling 5, 21-36.
Ohta, K., Yagi, T., Taketoshi, N., Hirose, K., Komabayashi, T., Baba, T., Ohishi, Y., Hernlund, J., 2012. Lattice thermal conductivity of MgSiO3 perovskite and post-perovskite at the core–mantle boundary. Earth and Planetary Science Letters 349–350, 109-115.
Osako, M., Ito, E., 1991. Thermal diffusivity of MgSiO3 perovskite. Geophysical Research Letters 18, 239-242.
Ould Lahoucine, C., Khellaf, A., 2004. Periodic method: Correction for thermocouple and simultaneous estimation of thermal conductivity and thermal diffusivity. Review of Scientific Instruments 75, 2356-2361.
Poirier, J.P., Peyronneau, J., Gesland, J.Y., Brebec, G., 1983. Viscosity and conductivity of the lower mantle; an experimental study on a MgSiO3 perovskite analogue, KZnF3. Physics of the Earth and Planetary Interiors 32, 273-287.

Salama, Y., Chennaoui, M., Sylla, A., Mountadar, M., Rihani, M., Assobhei, O., 2016. Characterization, structure, and function of extracellular polymeric substances (EPS) of microbial biofilm in biological wastewater treatment systems: a review. Desalination and Water Treatment, 57-35.

Scheper, T.H., Hilmer, J.M., Lammers, F., Müller, C., Reinecke, M., 1996. Biosensors in bioprocess monitoring. Journal of Chromatography A 725, 3-12.
Seltz, H., Dunkerley, F.J., DeWitt, B.J., 1943. Heat Capacities and Entropies of Molybdenum and Tungsten Trioxides. Journal of the American Chemical Society 65, 600-602.
Smith, D.F., Brown, D., Dworkin, A.S., Sasmor, D.J., Van Artsdalen, E.R., 1956. Low Temperature Heat Capacity and Entropy of Molybdenum Trioxide and Molybdenum Disulfide. Journal of the American Chemical Society 78, 1533-1536.
Strub, F., Castaing-Lasvignottes, J., Strub, M., Pons, M., Monchoux, F., 2005. Second law analysis of periodic heat conduction through a wall. International Journal of Thermal Sciences 44, 1154-1160.
Vojinović, V., Cabral, J.M.S., Fonseca, L.P., 2006. Real-time bioprocess monitoring: Part I: In situ sensors. Sensors and Actuators B: Chemical 114, 1083-1091.
Wallhäußer, E., Hussein, M.A., Becker, T., 2012. Detection methods of fouling in heat exchangers in the food industry. Food Control 27, 1-10.
Wirtanen, G.U.N., Mattila-Sandholm, T., 1993. Epifluorescence Image Analysis and Cultivation of Foodborne Biofilm Bacteria Grown on Stainless Steel Surfaces. Journal of Food Protection 56, 678-683.

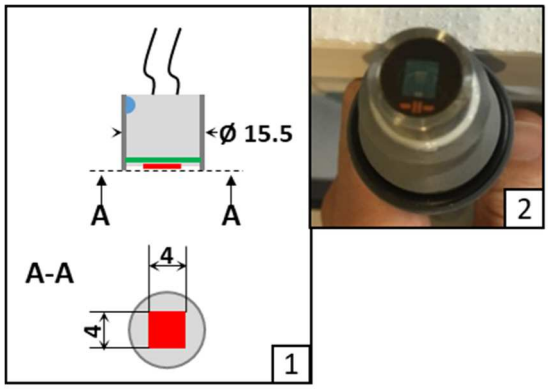

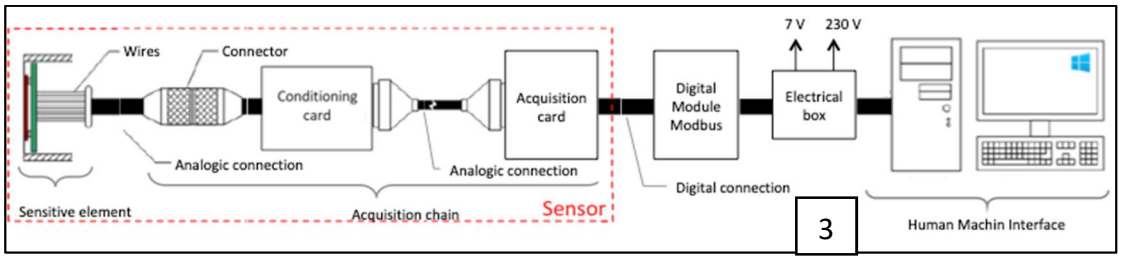

Figure 1: Scheme and picture of the sensor and its acquisition chain. 1: side and front view with dimensions, 2: picture of front side and 3: acquisition chain

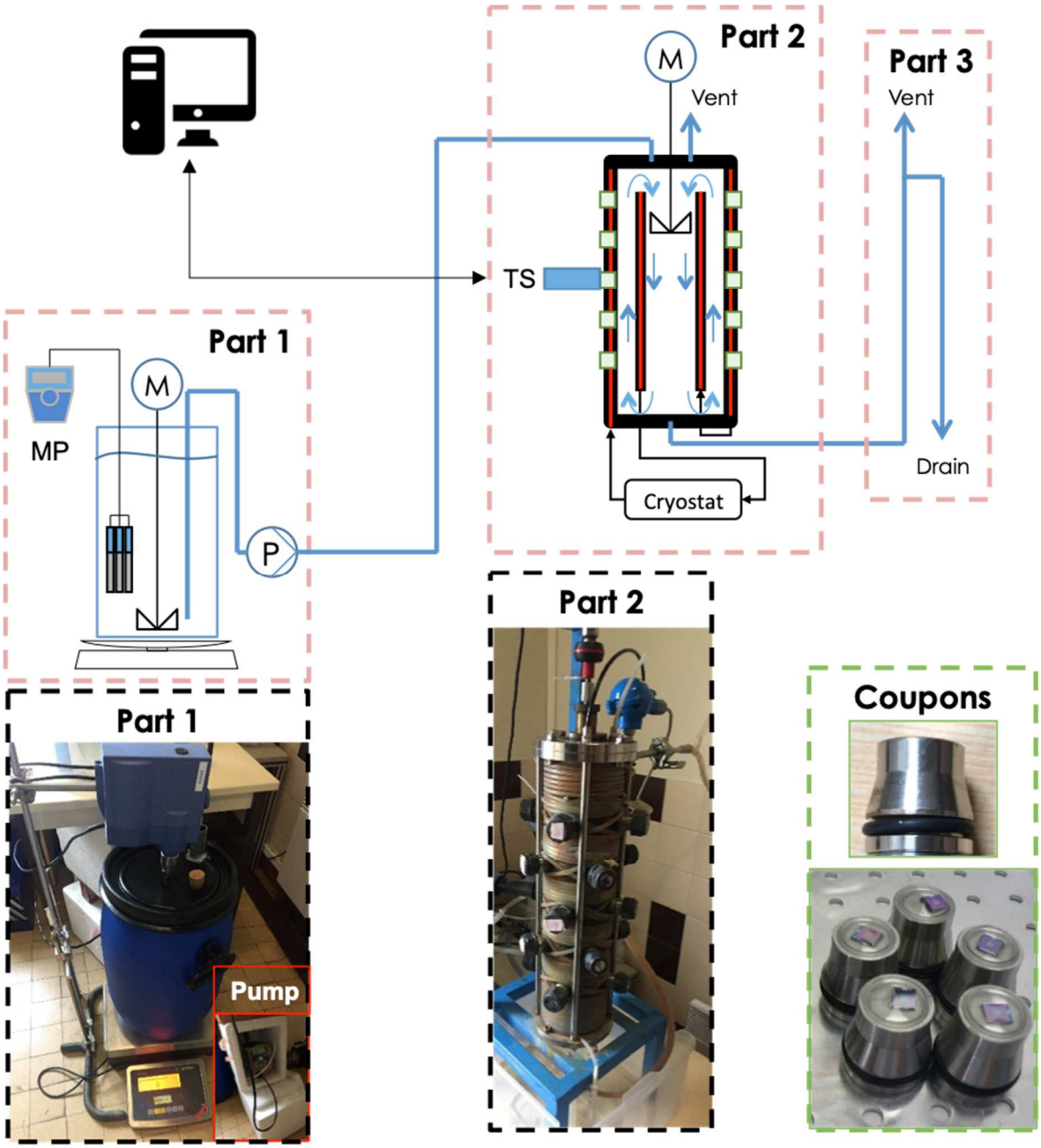

Figure 2: Scheme of the experimentation at pilot scale including part 1: feed tank with multi-parameter (MP), mixing, pump, Part 2: Propella™ reactor with 20 connections (for TS or coupons), cryostat (regulation and temperature measurement) and mixing, Part 3: drain with a ventilation opening. Pictures of parts 1, 2 and coupons.

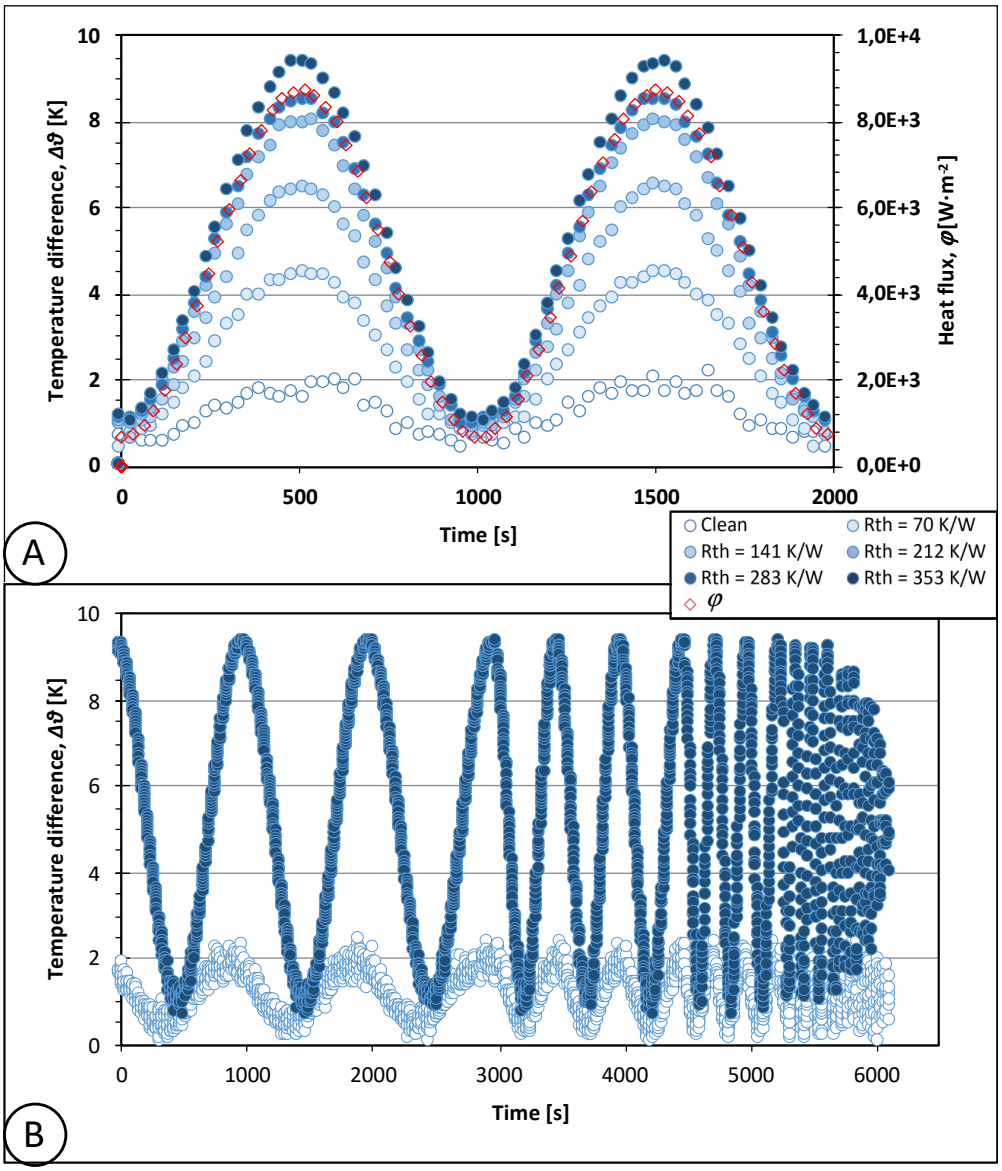

Figure 3: Raw data in PTR. (A) Temperature differences, $\Delta\theta$ and heat flux, φ versus time under clean and fouled (PVC adhesive tape, 700 µm) for f = 0.001Hz. (B) Concatenation of temperature differences from 0.001 to 0.2 Hz versus time in clean and fouled (PVC adhesive tape, 700 µm) conditions.

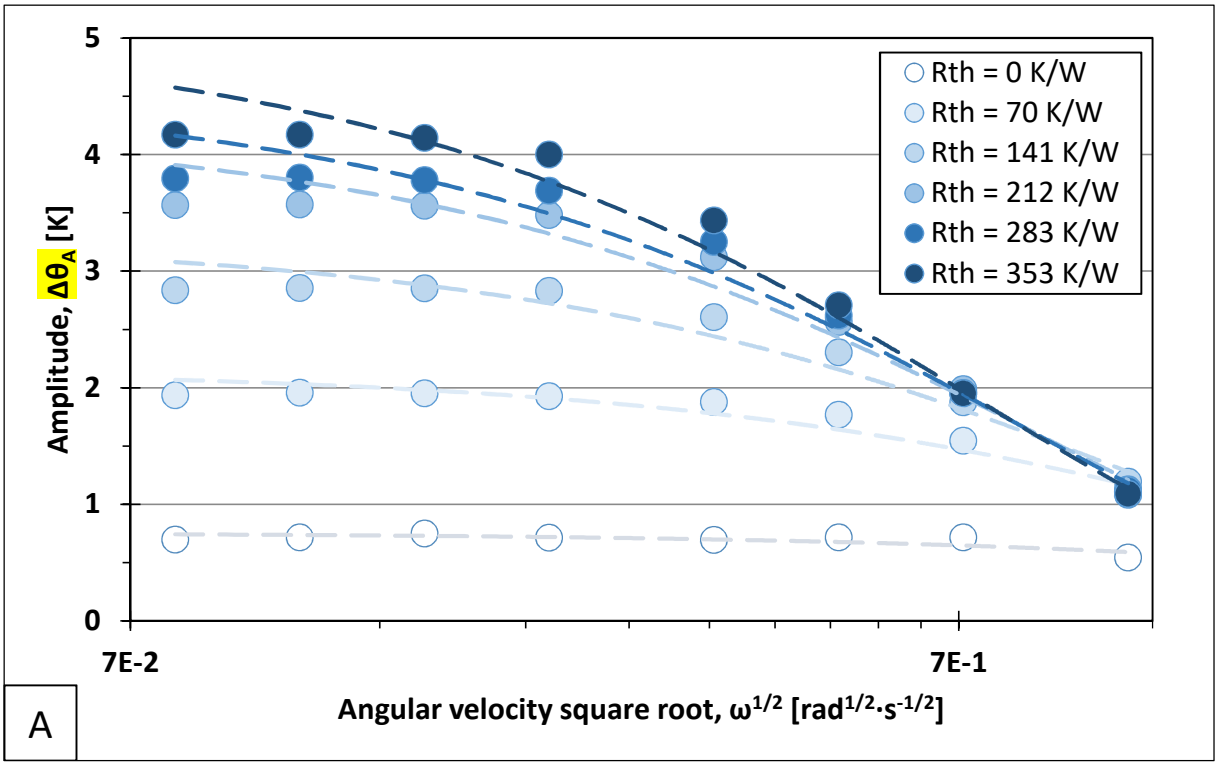

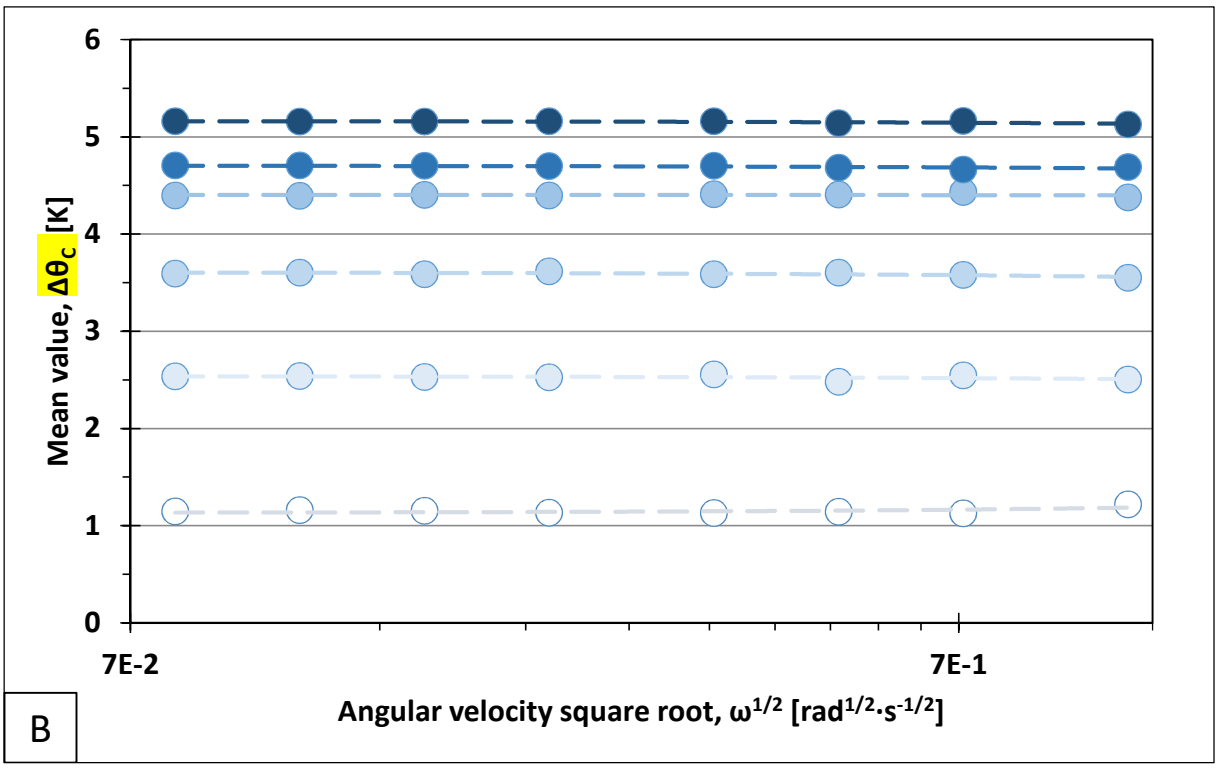

Figure 4: Amplitude (A) and mean temperature difference (B) versus angular velocity square root ($\omega = 2 \cdot \pi \cdot f$) in clean and fouled (PVC adhesive tape, up to 700 µm) conditions.

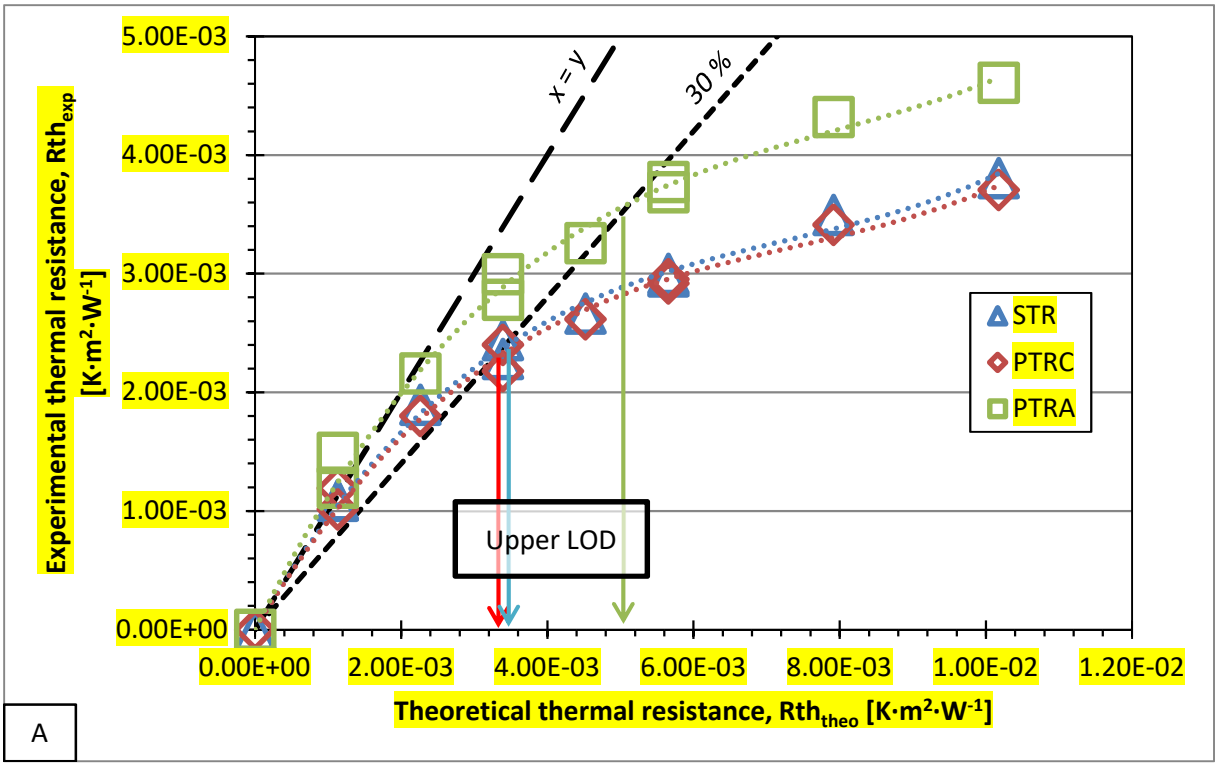

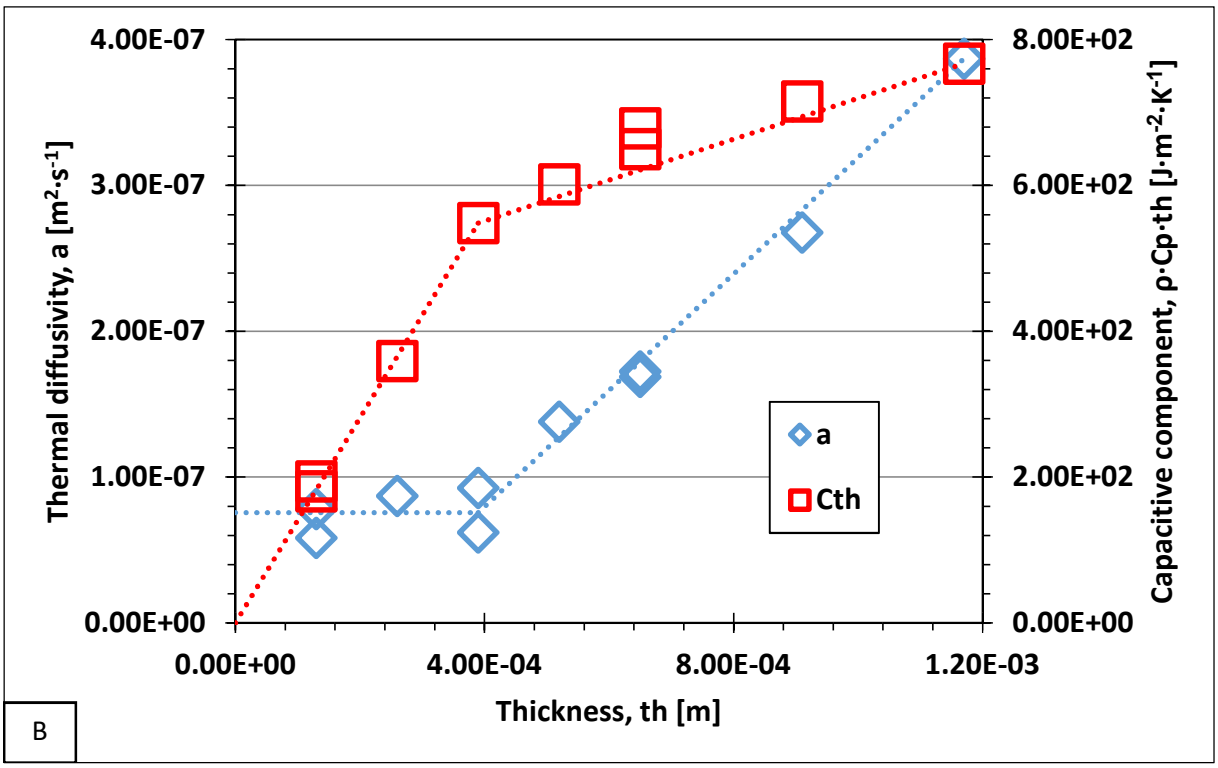

Figure 5 A) Experimental versus theoretical thermal resistances (PVC adhesive tape, from 0 to 1260 µm) in STR (Boukazia et al. 2020) and PTR (amplitude components and continuous temperature differences). B) Evolution of thermal diffusivity and capacitive component as a function of theoretical fouling thickness (PVC adhesive tape, from 0 to 1260 µm).

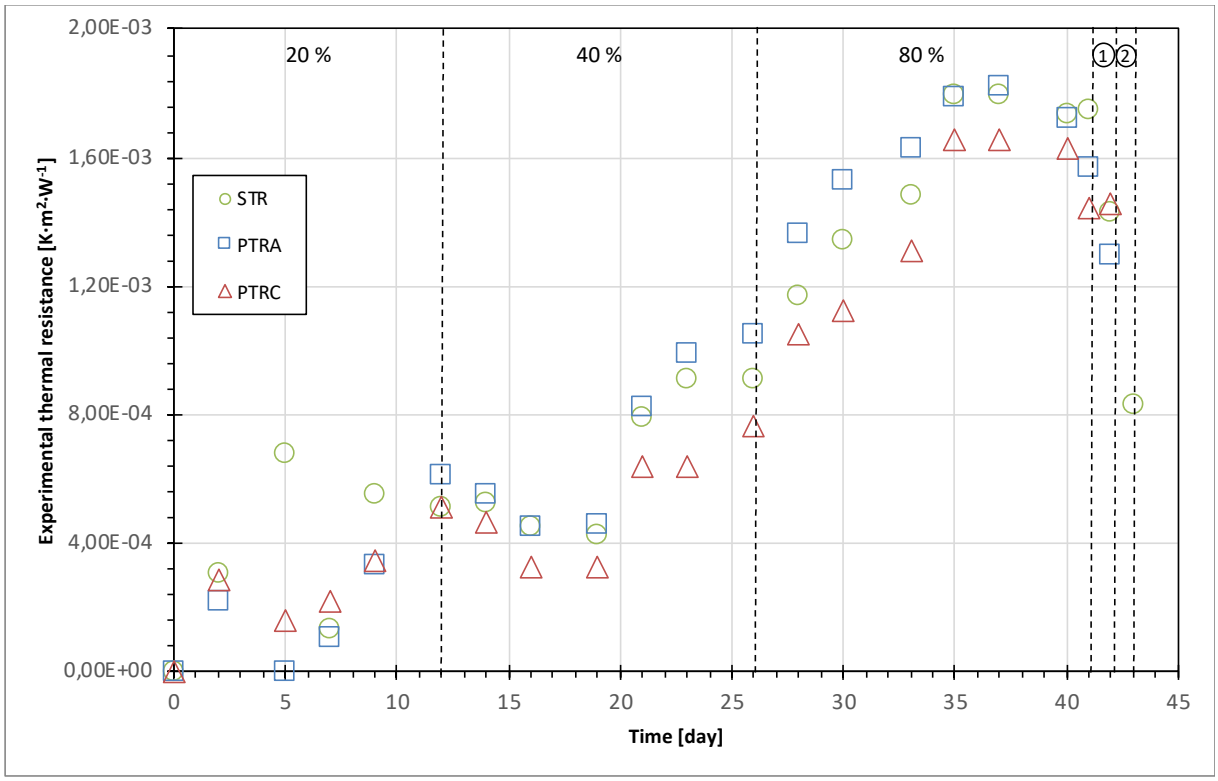

Figure 6: Experimental thermal resistance in STR, amplitude (PTR_A) and continuous temperature difference (PTR_C) in PTR as a function of operating time. ① First cleaning phase (solution of 0.1% active chlorine in 9.6 L) and ② second cleaning phase (active chlorine pulse of 100 mL).

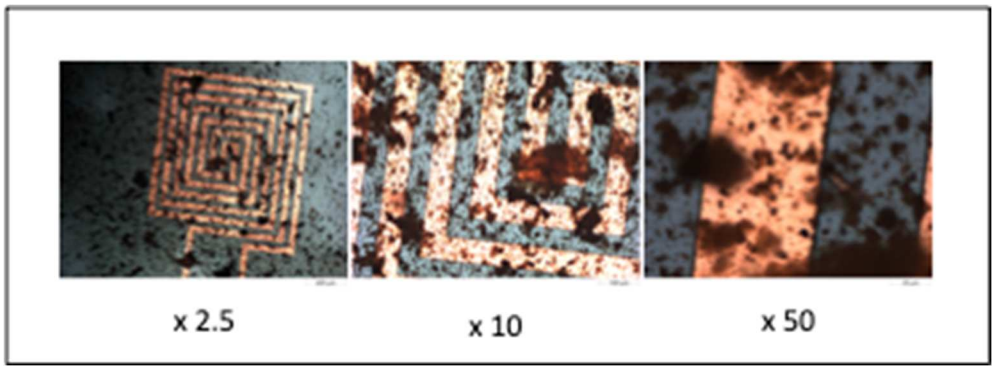

Figure 7: Observation of MEMS coupon surfaces after five weeks (magnifications x2.5 (1.12µm/pxl), x10 (0.28µm/pxl) and x20 (0.056µm/pxl), image size : 2584x2023pxl²).

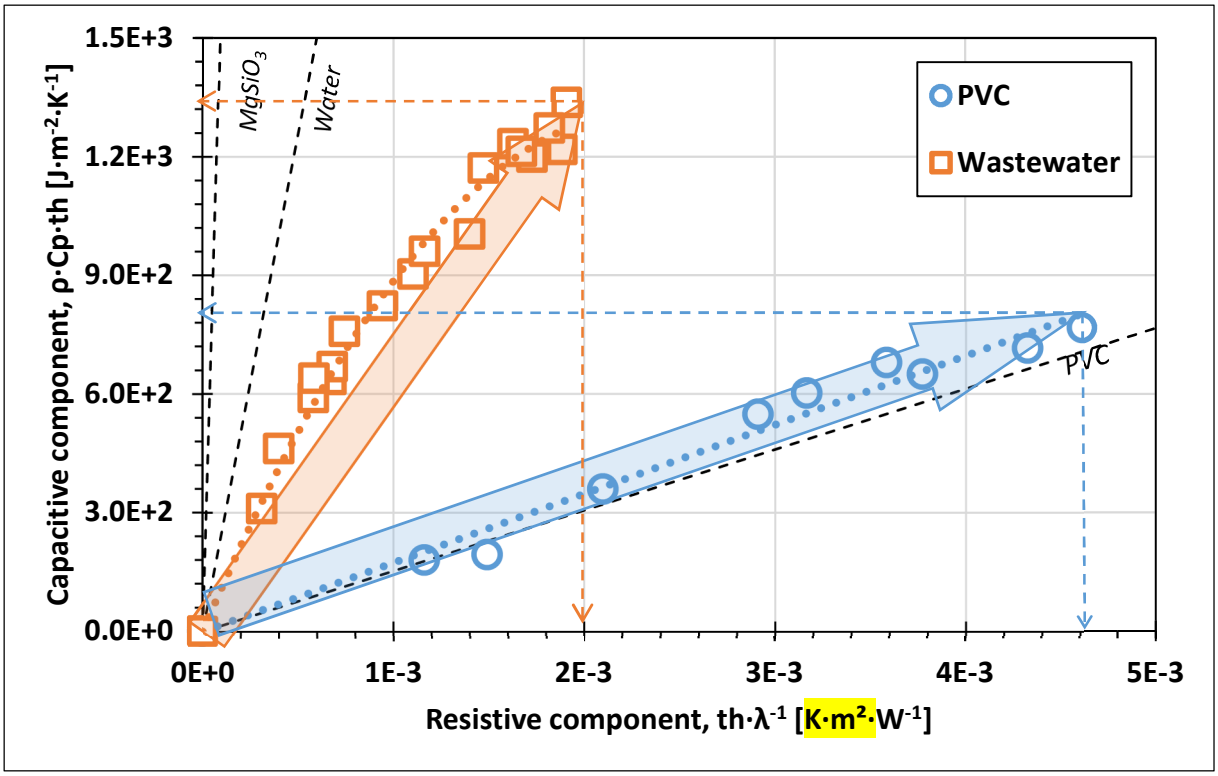

Figure 8: Fouling quantification and qualification in PTR. Evolution of capacitive component versus resistive component during (a) wastewater biofouling during 6 weeks at pilot-plant scale (Propella™, wastewater treatment) and (b) model fouling (PVC adhesive tape) at lab study (PVC adhesive tape). Data for magnesium silicate ($MgSiO_3$), water and PVC (doted lines) are reported from literature (Boukazia et al., 2020; Haigis et al., 2012).

Table 1: Amplitude and mean temperature differences in PTR (fouling conditions: PVC adhesive tape, from 0 to 700μm).

	Amplitude, $\Delta\theta_A$ [K]	**Mean, $\Delta\theta_C$ [K]**
Clean	$\boldsymbol{A_{\Delta\theta}} = 0.76exp(-0.22\omega^{0.5})$	$\overline{\Delta\theta} = 1.15$
R_{th} = 70 K·W^{-1}	$\boldsymbol{A_{\Delta\theta}} = 2.2exp(-0.55\omega^{0.5})$	$\overline{\Delta\theta} = 2.53$
R_{th} = 141 K·W^{-1}	$\boldsymbol{A_{\Delta\theta}} = 3.3exp(-0.84\omega^{0.5})$	$\overline{\Delta\theta} = 3.59$
R_{th} = 212 K·W^{-1}	$\boldsymbol{A_{\Delta\theta}} = 4.3exp(-1.1\omega^{0.5})$	$\overline{\Delta\theta} = 4.40$
R_{th} = 283 K·W^{-1}	$\boldsymbol{A_{\Delta\theta}} = 4.6exp(-1.2\omega^{0.5})$	$\overline{\Delta\theta} = 4.69$
R_{th} = 353 K·W^{-1}	$\boldsymbol{A_{\Delta\theta}} = 5.1exp(-1.3\omega^{0.5})$	$\overline{\Delta\theta} = 5.15$

Table 2: Relative deviation between thermal resistances in STR and PTR (fouling conditions: PVC adhesive tape, from 0 to 700µm)

	Relative deviation [%]	
R_{th_theo}	STR - PTR_C	PTRM - PTR_A
1,13E-03	7.11	16.2
2,26E-03	4.21	15.9
3,39E-03	1.22	17.6
4,52E-03	1.05	14.2
5,65E-03	0.43	13.0
Mean	2.80	15.4

Thermal Sensor

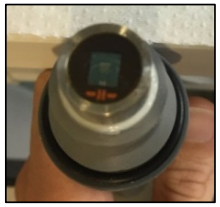

- MEMS
- Flat geometry
- Without protective layer

- 8 frequencies: 0.001 to 0.2 Hz

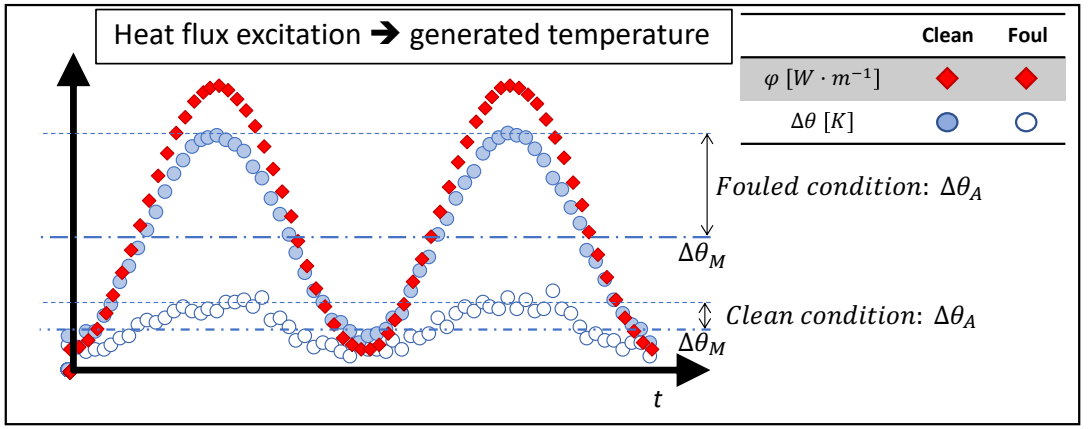

Scale	Fouling condition
Lab	PVC adhesive tape
Pilot-plant	Wastewater complex biofouling